Dynamics and Stability of Systems, Vol. 12, No. 3, 1997

Finite element analysis of the buckling and mode jumping of a rectangular plate

Jean-Jacques Gervais, Abderrahmann Oukit and Roger Pierre
Département de Mathématiques et de Statistique, Université Laval, Québec, Canada G1K 7P4

(Received February 1997; final version May 1997)

Abstract. *This paper presents the construction, validation and application of a toolkit which allows the combination of the well-understood theoretical analysis of the post-buckling behavior of a rectangular plate and of the numerical treatment of general boundary conditions. The construction is based on appropriate mixed finite element discretizations of both the spectral and nonlinear problems, with which one can obtain reliable approximations of the relevant parameters.*

1 Introduction

Consider a thin flat rectangular plate

$$\Omega = \{(x, y) | 0 \leq x \leq l, 0 \leq y \leq 1\}$$

subjected to a uniform compression applied in the normal direction to the vertical part of the boundary. Let u denote the vertical displacement of the median plane of the plate and

$$D_2 u = u_{x,x} \tag{1}$$

In view of studying large displacements, we shall assume that u is the first component of the solution of the von Kármán equations

$$\left.\begin{aligned} \Delta^2 u &= [u, \phi] - \lambda D_2 u \\ \Delta^2 \phi &= -\tfrac{1}{2}[u, u] \end{aligned}\right\} \tag{2}$$

where Δ^2 is the bilaplacian and $[\,.\,,\,.\,]$ is the Poisson bracket defined by

$$[u, v] = u_{x,x} v_{y,y} + u_{y,y} v_{x,x} - 2u_{x,y} v_{x,y} \tag{3}$$

The unknown ϕ is the Airy stress potential and λ is a measure of the applied compression. The system (2) must be supplemented with boundary conditions that correctly describe the physical state of the plane. For the displacement, we shall mainly consider three classical cases (here and henceforth the subscript n

E-mail: jjg@mat.ulaval.ca and rpierre@mat.ulaval.ca.

0268-1110/97/030161-25

denotes the derivative in the direction normal to the boundary):

- $I(u)$: simply supported on the whole boundary: $u = \Delta u = 0$ on $\partial\Omega$;
- $II(u)$: simply supported on the horizontal boundaries and clamped on the vertical: $u = \Delta u = 0$ at $y = 0$, $y = 1$ and $u = u_n = 0$ at $x = 0$, $x = l$;
- $III(u)$: clamped on the whole boundary: $u = u_n = 0$ on $\partial\Omega$.

The question of the appropriate boundary conditions for ϕ is not so clearly settled and the following possibilities are considered in the literature:

- $I(\phi)$: $\phi = \Delta\phi = 0$ on $\partial\Omega$;
- $II(\phi)$: $\Phi_n = (\Delta\phi)_n = 0$ on $\partial\Omega$;
- $III(\phi)$: $\phi = \phi_n = 0$ on $\partial\Omega$.

The physical relevance of these boundary conditions is at stake and a good case is made in Schaffer and Golubitsky (1979) for the choice $II(\phi)$. However, from the mathematical point of view, it is still interesting to consider the other possibilities (see Berger & Fife, 1968; Holder & Schaeffer, 1984; Potier-Ferry, 1978).

When the load λ exceeds a critical load λ_0, the plate buckles to a configuration with a certain wavenumber k (which is the number of zeros of the deflection along the median line $y = \frac{1}{2}$). In certain cases, as λ is further increased beyond λ_0, the plate undergoes a 'sudden and violent jump' to a new configuration with wavenumber $k + 1$. This is the so-called 'mode-jumping' phenomenon which was observed experimentally by Stein (1959).

From the mathematical point of view, the initial buckling is a bifurcation at λ_0 of non-trivial solutions from the trivial one $u = 0$ and several authors (Bauer *et al.*, 1975; Berger & Fife, 1968; Schaeffer & Golubitsky, 1979) have suggested that mode jumping occurs through a secondary bifurcation. As shown by Bauer *et al.* (1975), secondary bifurcations are often obtained by perturbing a bifurcation problem with a multiple eigenvalue (which in this context is double). However, as was clearly pointed out by Schaeffer and Golubitsky (1979), the sole presence of a double eigenvalue is not enough for the perturbed problem to exhibit mode jumping. In fact, they showed that the proper combination of double eigenvalues and boundary conditions is essential to model this phenomenon. In the above-mentioned work in a complementary paper by Holder and Schaeffer (1984), it is proved that mode jumping will occur with the following combinations of boundary conditions ($II(u)$, $I(\phi)$ or $II(\phi)$), but will not be observed with the choices ($I(u)$, $I(\phi)$ or $II(\phi)$).

Notwithstanding the discussions about the validity of boundary conditions for the stress potential, from the mathematical point of view, the only thing that precluded the analysis of other combinations of boundary conditions is the limitation of the mathematical toolbox used. Fourier analysis, which played a key role in those works, fails to give the exact form of the solutions in other cases or even the exact value of the critical length of the plate for which one indeed gets a double eigenvalue. To get around that difficulty, we have developed a numerical tool based on the use of a mixed finite element discretization which allows one to compute approximations of the critical length and of the corresponding spectral quantities, to determine the form of the associated bifurcation diagrams and finally to compute approximations of the so-called modal parameters, the value of which gives precise information about the occurrence of mode jumping.

Using this tool, we shall analyze the following combinations of boundary conditions which have not be treated by other means ($I(u)$ or $II(u)$, $III(\phi)$),

($III(u)$, $I(\phi)$ or $II(\phi)$ or $III(\phi)$). The resulting analysis will be detailed as follows: in Sections 2 and 3, we recall the necessary theoretical results; in Section 4, we present the finite element discretizations and discuss their appropriatness; and, in Section 5, we provide a sample of the numerical results thus produced.

2 The von Kármán equations and the associated eigenproblem

Before discussing the actual bifurcation problem, it will be useful to rewrite the von Kármán system as an operator equation $F(u, \lambda) = 0$. To do this, we shall need the fact that Δ^2 is invertible on the subspaces of $H^2(\Omega)$ that correspond to the various boundary conditions. For this, we define the inner product

$$(u, v) = \int_\Omega \Delta u \Delta v \, d\underline{x}$$

and the associated semi-norm

$$|u| = \left(\int_\Omega |\Delta u|^2 \, d\underline{x} \right)^{1/2}$$

On $H^2(\Omega) \cap H_0^1(\Omega)$ and hence on all closed subspaces, $|\cdot|$ defines a norm which is equivalent to the $H^2(\Omega)$-norm (Falk & Osborn, 1980). This ensures invertibility of Δ^2 on the spaces

$$V = \{\phi \in H^2(\Omega) | \phi = 0 \text{ on } \partial\Omega\}$$

$$V = \{\phi \in H^2(\Omega) | \phi = \phi_n = 0 \text{ on } \partial\Omega\}$$

which correspond to the boundary conditions $I(\phi)$ and $III(\phi)$, and also on

$$X = H^1(\Omega) \cap H_0^1(\Omega)$$

$$X = \{u \in H^2(\Omega) \cap H_0^1(\Omega) | u_n = 0 \text{ on } x = 0, x = l\}$$

$$X = \{u \in H^2(\Omega) | u = u_n = 0 \text{ on } \partial\Omega\} := H_0^2(\Omega)$$

This takes care of $I(u)$–$III(u)$. For the $II(\phi)$ case, one can prove invertibility on the quotient space

$$V = \{\phi \in H^2(\Omega) | \phi_n = 0 \text{ on } \partial\Omega\}/\mathbb{R}$$

with no loss of physical significance, by simply writing the inverse biharmonic operator as the square of the inverse Neumann operator (Schaeffer & Golubitsky, 1979). From now on, the index on Δ^2 will identify its domain. In view of the above, we may first rewrite $(2)_2$ as

$$\phi = -\frac{1}{2} \Delta_V^{-2} [u, u] \tag{4}$$

and obtain the desired form by substituting this in $(2)_1$:

$$F(u, \lambda) := u - \lambda \Delta_X^{-2} D_2(u) + \frac{1}{2} \Delta_X^{-2} [u, \Delta_V^{-2} [u, u]] = 0 \tag{5}$$

Now, we clearly have $F(0, \lambda) = 0$ for all λ and it is known that $u = 0$ is the only solution for $\lambda \leq \lambda_0$ where the critical value λ_0 is the smallest for which the tangent

operator $D_u F(0, \lambda)$ becomes singular. This is where the first bifurcation occurs. Our definition of λ_0 is equivalent to saying that it is the smallest solution of the eigenproblem

$$\Delta^2 w + \lambda D_2 w = 0, \qquad w \in X \tag{6}$$

which does not involve the stress potential ϕ. Our primary concern being the analysis of the mode jumping phenomenon, we shall be looking for the critical length l_c for which the minimal eigenvalue λ_0 is double.

The case $I(u)$ is classical. There the eigenvalues and eigenvectors can be computed for any length l and it is an easy matter to get the expressions of the critical quantity for $l = l_c$. The case $II(u)$ is not much harder. Although the expression of the eigenvalues is not accessible for $l \neq l_c$, if one uses the assumption that the first eigenvalue is double, one can get all the desired values in analytical form (Schaeffer & Golubitsky, 1979). In fact, it is a simple affair to write a Maple procedure to generate numerically the eigenvalues (which are roots of a nonlinear equation) and then to obtain the analytical expression of the eigenvectors. The main point here is that, in all the above calculations, one makes use of Fourier analysis which requires an *a priori* knowledge of the form of the eigenvectors. This approach fails for the case $III(u)$ and it does not seem to be possible to get the analytical form of any of the critical quantities. This is where discretization will get into the picture.

3 The mixed finite element approximations and the numerical solver

In this section, we discuss the approximations and algorithms that have been used to solve three different but related problems, namely the nonlinear problem (2), its linear counterpart

$$\Delta^2 w = f, \qquad \text{in } \Omega \tag{7}$$

and the eigenproblem (6). In all three cases, we have chosen a mixed finite element discretization of the type discussed in Falk and Osborn (1980), in order to get around the difficulties that are met in the construction of conformal approximations of $H^2(\Omega)$. The underlying idea is classical: one introduces an auxiliary variable on which part of the regularity and of the boundary conditions are transferred. The relation between this new variable and the primary one is then treated as a constraint and the resulting variational problem corresponds to some saddle point formulation. The specifics are discussed in the following.

3.1 The resolution of the linear problem

In order to solve (7), the simplest choice that can be made of an auxiliary variable is $\psi = \Delta w$. The corresponding weak formulation is: find $(\psi, w) \in H \times W$ such that

$$\begin{aligned} &\int_\Omega \psi \mu \, d\underline{x} + \int_\Omega \nabla \mu \cdot \nabla w \, d\underline{x} = 0, \qquad \forall \mu \in H \\ &\int_\Omega \nabla \psi \cdot \nabla v \, d\underline{x} + \int_\Omega f v \, d\underline{x} = 0, \qquad \forall v \in W \end{aligned} \tag{8}$$

where the spaces H and W are chosen in accordance with the boundary conditions. In the $III(u)$ case, one chooses $H = H^1(\Omega)$, $W = H_0^1(\Omega)$ and it is a simple

exercise to verify that, if the pair (ψ, w) is a solution of (8), then w is a solution of (7) which is zero on Γ. The condition $w_n = 0$ on Γ is no longer imposed and becomes a natural boundary condition that is deduced from $(8)_1$. The question of the existence of such a solution is not straightforward, but can be settled with the help of known regularity results (see Falk & Osborn, 1980). To discretize (8), we construct a triangulation $\mathcal{T}_h$ of Ω (here h is the discretization parameter), and define conformal approximations H_h and W_h of H and W, using C^0 triangular element of degree 2, for which good approximation results can be obtained (Falk & Osborn, 1980).

The treatment of simply supported boundary conditions is also straightforward: the natural condition $\Delta w = 0$ becomes an essential boundary condition on ψ. Thus, the correct choice is now $H = W = H_0^1(\Omega)$ with appropriate transfer at the finite element level.

The case of boundary conditions $II(\phi)$ requires more comments. As pointed out in Section 2, in this case, the operator Δ^{-2} can be factored into a product of inverse Neumann operators, thus one expects that compatibility conditions will have to be satisfied. These are precisely

$$\int_\Omega f \, d\underline{x} = \int_\Omega \psi \, d\underline{x} = 0$$

Now, the mixed formulation is again (8) where $W = H^1(\Omega)$. The compatibility condition

$$\int_\Omega \psi \, d\underline{x} = 0$$

follows directly from the first equation and, if f satisfies the first one, we will get the correct solution. The difficulty here stems from the discretization. Whatever the quadrature used to compute the source term, it will amount to approximating f by some polynomial $\pi_h(f)$. But, the fact that the average of f on Ω is zero, does not imply that the same is true for $\pi_h(f)$, hence we might stumble on a ill-posed discrete problem. We thus have to define some generalized inverse. In the finite element context the simplest way to do so is to replace, in $(8)_2$, the term $\int_\Omega fv \, d\underline{x}$ by $\int_\Omega (f - \mu(f))v \, d\underline{x}$ where $\mu(f)$ is the L^2-projection of f on to the constants (i.e. its average on Ω). Any quadrature, of order greater than zero, will commute with this projection (i.e. $\mu(\pi_h(f)) = (\pi_h(\mu(f)))$) and the solution of the discrete problem will converge to the solution of the continuous one.

3.2 The computation of the spectral quantities

Formulation (8) is also the one that we have used to solve the eigenproblem (6). The way to do it is simply to modify the second equation by replacing the source term by

$$-\lambda \int_\Omega \frac{\partial u}{\partial x} \frac{\partial v}{\partial x} \, d\underline{x}$$

The use of such a formulation to solve eigenvalue problems related to the plate problem (7) is considered in Babŭska and Osborn (1991), although in a slightly simpler form. The analysis presented therein could be modified to cover the cases

treated here. We shall not present this modification and shall satisfy ourselves by validating the resulting code on known cases.

This code has been used for two different purposes: first, to determine the critical length at which the first bifurcation corresponds to a double eigenvalue and, next, to compute the corresponding eigenvectors. Because the length is not known *a priori*, it is not practical to work on the domain Ω itself, since this would force a re-meshing each time the length is changed. Instead, we perform a change of spatial variables

$$\hat{x} = \frac{x}{l}, \qquad \hat{y} = y, \qquad \forall (x, y) \in \Omega \tag{9}$$

The resulting problem is now set on $[0, 1]^2$ but with variational forms containing coefficients depending on l. Finally, the finite element formulation of the spectral problems is obtained by using the same discretization as in the preceding section. According to Babŭska and Osborn (1991), one can hope for a h^2 convergence of both the eigenvalues and the eigenvectors (in the L^2-norm). From the practical point of view, this means that reliable values can be expected on a medium size mesh and this is what we observed (see Section 5.1). The necessary meshes are constructed once and for all but, each time the length is modified, the finite element matrix is rebuilt, stored in skyline form and factorized in the same storing space.

We are thus left, for each length l, with the problem of computing the smallest eignevalue of a large matrix. To be more precise, let us rewrite this eigenproblem in matrix form

$$\begin{pmatrix} \mathbf{M} & \mathbf{B}^t \\ \mathbf{B} & 0 \end{pmatrix} \begin{pmatrix} \Psi \\ U \end{pmatrix} = \lambda \begin{pmatrix} 0 \\ DU \end{pmatrix} \tag{10}$$

where $\mathbf{M}$ is the matrix of the L^2 inner product on the finite element space, $\mathbf{B}$ the matrix representing the Dirichlet integral and D is the discretization of the operator D_2. If we eliminate Ψ from (10), we are led to the following discrete version of (6)

$$\mathbf{B}\mathbf{M}^{-1}\mathbf{B}^t U + \lambda DU = 0 \tag{11}$$

In (11), the matrix is symmetric positive definite and, if it was sparse, we could use any of the good eigensolvers currently available in numerical libraries. However, the matrix $\mathbf{M}^{-1}$ is full and thus the matrix in (11) cannot be stored economically. Because of that, we have to resort to an approach which does not require the use of the matrix itself. In a recent paper, Duff and Scott (1991) have proposed a coupling of the subspace iteration method to a Tchebychev acceleration technique, resulting in an efficient general eigensolver named EB12 and written in FORTRAN 77. One can benefit from the acceleration if the eigenvalues that are sought are either the rightmost or the leftmost in the complex plane. In our case, the eigenvalues being real, the biggest ones of the inverse matrix are also its rightmost and these are the ones that we looked for. The method is fully described in Duff and Scott (1991) so that we shall limit ourselves to one more comment. The only thing that the code EB12 leaves to be performed by the user is the matrix vector products, which, in our case, are written

$$\mathbf{V} = -(\mathbf{B}\mathbf{M}^{-1}\mathbf{B}^t)^{-1} DU$$

Because of the storage limitations quoted above, the corresponding linear problem cannot be solved in that form and one has to revert the process leading from (10)

to (11) and go back to the mixed form even if the variable Ψ is of no interest here. Thus, in order to use the code of Duff and Scott, the only thing that we have to do is to couple EB12 to the finite element program used to solve (8).

The approximation of the eigenpairs is then done in two steps: first, we compute the eigenvalues and a basis of the eigenspace using EB12ab and, then from that basis, we call EB12bd to compute the eigenvectors in the required order. More information on the relevant numerical parameters will be given later.

3.3 The resolution of the nonlinear problem

Apart from the nonlinearity, the main difference between the von Kármán equations problem and the plate problem (7) is the appearance of the Poisson bracket. To see how this will be treated with a mixed formulation, we first go back to the linear case. An alternative to the mixed formulation (8) is obtained by choosing as auxiliary variable the full Hessian tensor $\underline{\underline{\sigma}} = \nabla^2 w$. This possibility is particularly interesting if one has to solve the plate problem on non-polygonal geometries. In that case the value of the Poisson ratio (which is absent here) has to be taken into account and the bending energy functional depends on all of the second-order derivatives of the displacement through the Poisson bracket, in exactly the same way as in the von Kármán system. In our context, i.e. (7), the new mixed variational formulation is written as

$$\left.\begin{aligned} &\int_\Omega \underline{\underline{\sigma}} : \underline{\underline{\mu}}\, d\underline{x} + \int_\Omega \operatorname{div} \underline{\underline{\mu}} \cdot \nabla w\, d\underline{x} = 0, \qquad \forall \underline{\underline{\mu}} \\ &\int_\Omega \operatorname{div} \underline{\underline{\sigma}} \cdot \nabla v\, d\underline{x} + \int_\Omega f v\, d\underline{x} = 0, \qquad \forall v \end{aligned}\right\} \tag{12}$$

This formulation, due to Miyoshi (1976), has been studied in Falk and Osborn (1980) and more recently in Oukit and Pierre (1996). In this last work, it was shown that, to have good approximation properties with triangular elements, one has to use polynomial spaces of order at least 2 and this is what we have chosen here.

The implementation of the various boundary conditions requires some care. As one would expect, the Dirichlet condition $w = 0$ is imposed in the displacement space and the condition $\Delta w = \operatorname{tr}(\nabla^2 w) = 0$ is imposed in the tensor space.

The analysis of the other boundary conditions is based on a more general Green's formula, namely

$$\int_\Omega \underline{\underline{\mu}} : \underline{\underline{\varepsilon}}(\underline{v})\, d\underline{x} + \int_\Omega \operatorname{div}(\underline{\underline{\mu}}) \cdot \underline{v}\, d\underline{x} = \int_\Gamma (\underline{\underline{\mu}} \cdot \underline{n}) \cdot \underline{v}\, d\sigma \tag{13}$$

If we apply (13) to the first equation in (12), we deduce, in a standard way, that the behavior of the solution on the boundary is translated into the variational condition:

$$\int_\Gamma (\underline{\underline{\mu}} \cdot \underline{n}) \cdot \nabla w\, d\sigma = 0, \qquad \forall \underline{\underline{\mu}} \tag{14}$$

But, the domain being rectangular, $w = 0 \Rightarrow \partial w / \partial \tau = 0$ (where τ is the unit

tangent), hence, when $w = 0$ is imposed, (14) simplifies into

$$\int_\Gamma [(\underline{\underline{\mu}} \cdot \underline{n}) \cdot \underline{n}] \frac{\partial w}{\partial n} \, d\sigma = 0, \qquad \forall \underline{\underline{\mu}} \tag{15}$$

Thus, we again recover $\partial w/\partial n = 0$ as a natural boundary condition on the part of the boundary where $\underline{\underline{\mu}}$ is free. However, on the simply supported parts, the situation is a little different. It is not enough to impose $\operatorname{tr} \underline{\underline{\mu}} = 0$ there, because this does not imply $(\underline{\underline{\mu}} \cdot \underline{n}) \cdot \underline{n} = 0$. A simple algebraic computation shows that, in our geometry, the combination of the two requirements, $\operatorname{tr} \underline{\underline{\mu}} = (\underline{\underline{\mu}} \cdot \underline{n}) \cdot \underline{n} = 0$ leads to the boundary condition

$$\underline{\underline{\mu}}_{1,1} = \underline{\underline{\mu}}_{2,2} = 0, \qquad \forall \underline{\underline{\mu}} \tag{16}$$

Similarly if $w = 0$ is not imposed (as in the $II(\phi)$ case), the only way that we can recover $\partial w/\partial n = 0$ as a natural condition is to impose that the coefficient of $\partial w/\partial \tau$ be zero in (14). This coefficient is $(\underline{\underline{\mu}} \cdot \underline{n}) \cdot \underline{\tau}$ and, in our geometry, the corresponding condition is $\underline{\underline{\mu}}_{1,2} = 0$. Finally, the treatment of the boundary condition $\partial \Delta w/\partial n = 0$ is done as in the case (8). Indeed, applying Green's formula to the second equation of (12), one may check that, on the part of the boundary where v is left free, this condition is recovered as a natural boundary condition.

We now turn our attention to the von Kármán system itself. For this, we follow the presentation of Reinhart (1982) to which the reader is referred for the technical points. First, let $[[\cdot, \cdot]]$ denote the indefinite symmetric product of tensors defined by

$$[[\underline{\underline{\tau}}, \underline{\underline{\mu}}]] = \underline{\underline{\tau}}_{1,1}\underline{\underline{\mu}}_{2,2} + \underline{\underline{\tau}}_{2,2}\underline{\underline{\mu}}_{1,1} - 2\underline{\underline{\tau}}_{1,2}\underline{\underline{\mu}}_{1,2} \tag{17}$$

It may be checked that, for Hessians, this product corresponds to the Poisson bracket, i.e.

$$[[\nabla^2 v, \nabla^2 w]] = [v, w]$$

Following Ciarlet and Rabier (1980) we introduce the function $\theta_0 = -\frac{1}{2}x^2$ which satisfies

$$[\theta_0, v] = -D_2 v, \qquad \forall v$$

Next we set $\underline{\underline{\sigma}}_0 = \nabla^2 \theta_0$.

Taking the above into account, we can show that the introduction of the auxiliary variables $\underline{\underline{\sigma}}_u = \nabla^2 u$ and $\underline{\underline{\sigma}}_\phi = \nabla^2 \phi$ into (2) leads to the following system of nonlinear variational equations: find $(u, \underline{\underline{\sigma}}_u, \phi, \underline{\underline{\sigma}}_\phi)$ such that

$$\left.\begin{aligned}
\int_\Omega \underline{\underline{\sigma}}_u : \underline{\underline{\mu}} \, d\underline{x} + \int_\Omega \operatorname{div}(\underline{\underline{\mu}}) \cdot \nabla u \, d\underline{x} &= 0, \qquad \forall \underline{\underline{\mu}} \\
\int_\Omega \operatorname{div}(\underline{\underline{\sigma}}_u) \cdot \nabla v \, d\underline{x} + \int_\Omega (\lambda [[\underline{\underline{\sigma}}_0, \underline{\underline{\sigma}}_u]] + [[\underline{\underline{\sigma}}_u, \underline{\underline{\sigma}}_\phi]] + f) v \, d\underline{x} &= 0, \qquad \forall v \\
\int_\Omega \underline{\underline{\sigma}}_\phi : \underline{\underline{\mu}} \, d\underline{x} + \int_\Omega \operatorname{div}(\underline{\underline{\mu}}) \cdot \nabla \phi \, d\underline{x} &= 0, \qquad \forall \underline{\underline{\mu}} \\
\int_\Omega \operatorname{div}(\underline{\underline{\sigma}}_\phi) \cdot \nabla v \, d\underline{x} - \int_\Omega ([[\underline{\underline{\sigma}}_u, \underline{\underline{\sigma}}_u]]) v \, d\underline{x} &= 0, \qquad \forall v
\end{aligned}\right\} \tag{18}$$

A priori, $f = 0$. The case $f \neq 0$ would correspond to a vertical load and the introduction of such a term in the system is the appropriate way of obtaining a perturbed bifurcation diagram. The treatment of the boundary conditions is the same for (18) as for (12) and so is the discretization for which we again use triangular elements of degree 2. The validity of this choice is studied in Reinhart (1982) where it is shown that any discretization which is convergent for (12) will also be convergent for the regular solution of (18). Even limit and bifurcation points can be analyzed using the methodology of Brezzi *et al.* (1980–1981). This will be enough for our purpose.

In order to obtain a correct description of the bifurcation diagram of (2), we have worked on the discrete nonlinear system resulting from the discretization of (18). To avoid branching, we have used a perturbation–continuation algorithm that can be schematized as follows: to represent the diagram in the neighborhood of a bifurcation point,

- introduce a perturbation $f = \delta f_0$ where δ is a (small) numerical parameter and f_0 is a function which has the symmetry property of the solutions which are on the branch that we want to draw;
- follow the resulting perturbed branch using the Euler–Newton arc length continuation method of Keller (1977), as described in Glowinski *et al.* (1985) (from A to B);
- when far enough on the perturbed branch, set $f = 0$ and jump back on the non-perturbed branch (from B to C);
- trace back the non-perturbed branch using the same continuation procedure (from C to D).

Figure 1 gives a correct idea of the procedure and illustrates the fact that, with this approach, the only singular points that are encountered are either limit or pitchfork bifurcation points.

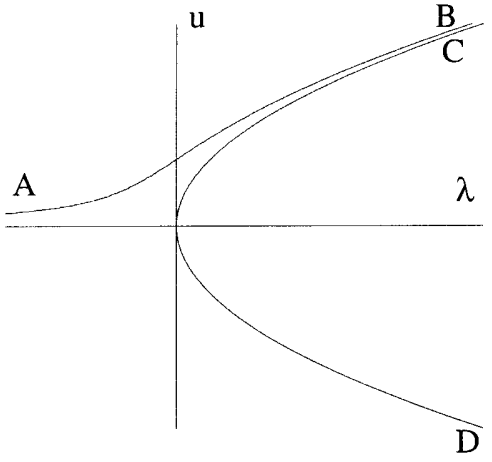

Fig. 1. The perturbation–continuation algorithm.

This approach is very costly. In fact, at each continuation step, we have to solve a nonlinear problem using a Newton method. Each Newton step will then require the solution of two linear systems (because λ is also an unknown) for which the matrix is the tangent matrix of (18) which will have to be assembled and factorized before resolution. An alternative to this approach is the use of an iterative method of the conjugate gradient type, but the results of Reinhart (1982) show that convergence is bound to be slow in the neighborhood of a limit point. It must be pointed out that the meshes used in Reinhart (1982) are rather coarse and that this problem could very well be worst on finer meshes, such as those used here. We believe that the question of designing an efficient iterative solver for the Keller continuation procedure is still open and this is why we stuck to Newton's method which, although expensive, is nevertheless very robust in that the number of iterations remains rather small even in the critical regions.

4 Results from singularity theory

We assume here that l_c is a critical length for which the minimal eigenvalue λ_0 is double. Using the Lyapunov–Schmidt reduction method and singularity theory, Golubitsky and Schaeffer (1979) have proved that the set of solutions near $(0, \lambda_0)$ of the von Kármán equations is qualitatively equivalent to the set of solutions near $(0, 0, 0)$ of the system of equations (in this section, (x, y) do not represent the spatial coordinates on the plate but the amplitudes of the solution in the space generated by the eigenvectors; since this change of notation is limited to this section, it should not create any confusion)

$$\left.\begin{aligned} x^3 + \mu x y^2 - \lambda x = 0 \\ \nu x^2 y + y^3 - \lambda y = 0 \end{aligned}\right\} \tag{19}$$

where we have replaced λ by $\lambda + \lambda_0$. Now, let w_1 and w_2 be the eigenvectors associated with the double eigenvalue λ_0. As we shall see later, w_1 and w_2 have consecutive wavenumbers, let us say k and $k+1$. For each pair (i, j), $i = 1, 2$, $j = 1, 2$ define ψ_{ij} to be the first component of the solution of (8) when $f = [w_i, w_j]$ and the boundary conditions are those imposed on the Airy potential. The coefficients in (19) are defined as follows:

$$\begin{aligned} a &= \tfrac{1}{2}\|\psi_{1,1}\|^2_{L^2}, & b &= \tfrac{1}{2}[2\|\psi_{1,2}\|^2_{L^2} + (\psi_{1,1}, \psi_{2,2})_{L^2}] \\ c &= \tfrac{1}{2}\|\psi_{2,2}\|^2_{L^2} \\ p &= \left\|\frac{\partial w_1}{\partial x}\right\|^2_{L^2}, & q &= \left\|\frac{\partial w_2}{\partial x}\right\|^2_{L^2} \\ \mu &= \frac{bq}{cp}, & \nu &= \frac{bp}{aq} \end{aligned} \tag{20}$$

The system (19) has the so-called $\mathbb{Z}_2 \otimes \mathbb{Z}_2$-symmetry, that is $(19)_1$ is odd in x and even in y while $(19)_2$ has the inverse parity. This symmetry property is inherited from the following symmetries of the von Kármán equations for a rectangular plate: the reflection through the plane of the plate, the reflection through the shortest median and the composition of these two reflections.

If we allow small perturbations of the von Kármán system that preserve these symmetries, Golubitsky and Schaeffer have proved that the perturbed equations

will be qualitatively equivalent to

$$\left.\begin{aligned} x^3 + \mu x y^2 - \lambda x &= 0 \\ \nu x^2 y + y^3 - (\lambda + \sigma) y &= 0 \end{aligned}\right\} \tag{21}$$

for a σ near 0 if (μ, ν) belongs to one of the regions 1–5 given in Fig. 2.

We may think of σ as $l - l_c$. This relation is rigorously established in Schaeffer and Golubitsky (1979). So all the small perturbations of the von Kármán equations preserving the preceding symmetries are obtained by slight perturbations l of l_c.

Let us describe the bifurcation diagram (i.e. the solution set in the (x, y, λ)-space) of the system (21). There are four types of solutions:

(1) $x = 0; y = 0$ (trivial solution)

(2) $y = 0; x^2 = \lambda$ (x-mode solution)

(3) $x = 0; y^2 = \lambda + \sigma$ (y-mode solution)

(4) $\left.\begin{aligned} \lambda &= x^2 + \mu y^2 \\ \lambda &= \nu x^2 + y^2 - \sigma \end{aligned}\right\}$ (mixed-node solution)

An x-mode solution corresponds to a solution with wavenumber k while a y-mode solution has a wavenumber equal to $k + 1$. For our purposes, it is sufficient to consider (μ, ν) in region 1 or 3. In Figs 3 and 4, we have, most of the time, drawn the part of the bifurcation diagrams in the quarter space $x \geq 0$, $y \geq 0$. The other parts are obtained via reflections through the planes $x = 0$ and $y = 0$.

For those diagrams corresponding to $\sigma \neq 0$, the dashed lines indicate unstable solutions and the stable ones are drawn as solid lines. These stability assignments are obtained as follows. When $\sigma \neq 0$, each bifurcation is either a sub-critical or a super-critical pitchfork bifurcation for which we have the standard exchange of stability property (see, for example, Golubitsky & Schaeffer, 1985, Chapter X). We shall comment on the behavior of the system when we have a bifurcation diagram such as the one depicted in Fig. 4(a), which is the most relevant for our study. For $\lambda < 0$ (we remind the reader that we have replaced λ by $\lambda + \lambda_0$), the system follows the trivial path (i.e. no deflection). As λ is increased (quasi-statically) past 0, the trivial solution becomes unstable and the system will follow the

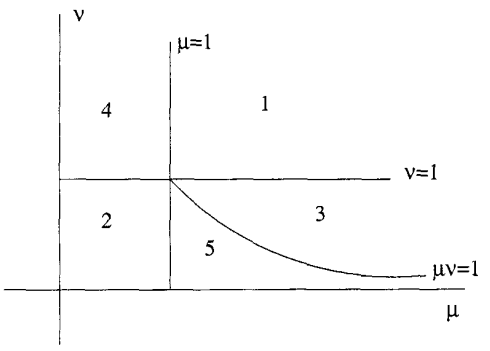

Fig. 2. Critical regions for the modal parameters.

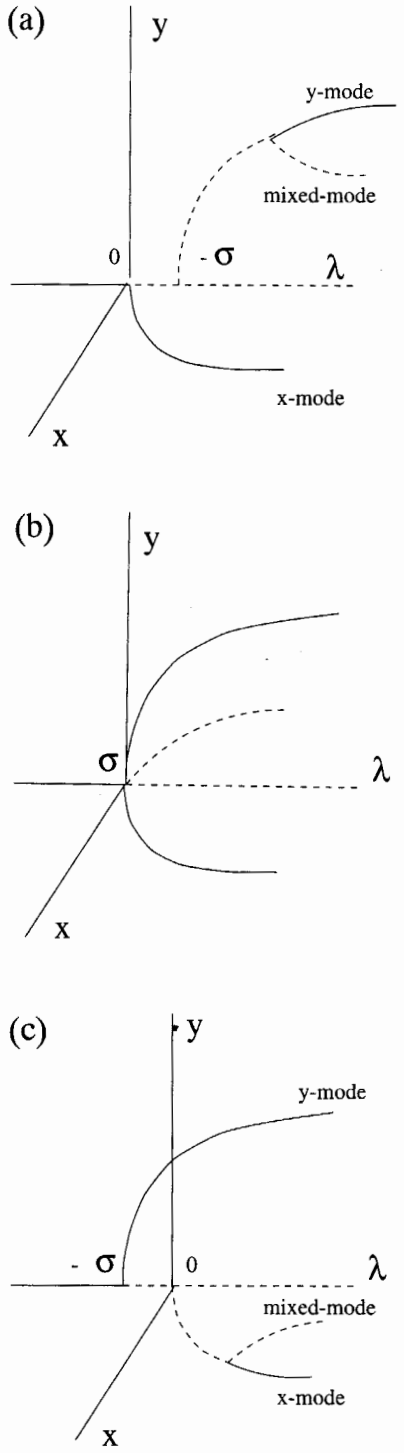

Fig. 3. Region 1: (a) $\sigma < 0$; (b) $\sigma = 0$; (c) $\sigma > 0$.

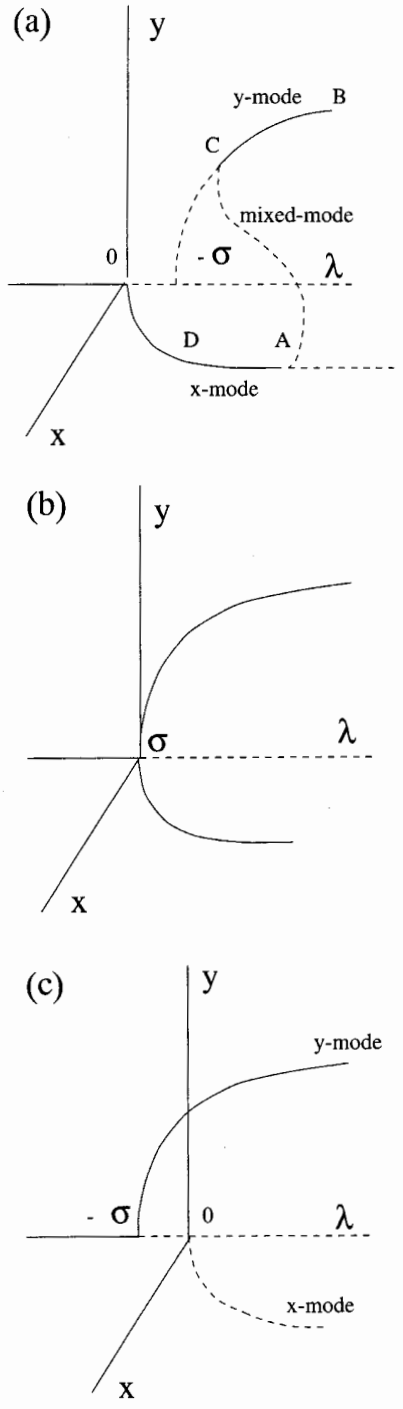

Fig. 4. Region 3: (a) $\sigma < 0$; (b) $\sigma = 0$; (c) $\sigma > 0$.

x-mode path (i.e. buckled state with wavenumber k) until the point A is reached where the x-mode solution loses its stability through a sub-critical pitchfork bifurcation. So, if λ is further increased the system makes a rapid transition presumably to the y-mode branch (i.e. buckled state with wavenumber $k+1$) at point B. This is in agreement with Stein's experiment. From this bifurcation diagram of steady solutions, we can predict a mode jumping, but we cannot predict with certainty that the dynamic behavior will be a jump from A to B, because the existence of other stable steady solutions, for the same range of λ, cannot be ruled out. For an approach using dynamics for the modelling of mode jumping phenomena, we refer the reader to Riks *et al.* (1996).

Schaeffer and Golubitsky (1979) and Holder and Schaeffer (1984) used Fourier analysis to evaluate μ and ν via the formulae (20) and concluded that mode jumping will occur with the combinations of boundary conditions ($II(u)$, $II(\phi)$) and ($II(u)$, $I(\phi)$) but will not be observed with the choices ($I(u)$, $I(\phi)$) or ($I(u)$, $II(\phi)$).

To be able to consider other combinations of boundary conditions, the only thing that we have to do is to show how the value of the same parameters can be obtained from our approximations. We assume that l_c has been determined, that the mesh is fixed and that we have assembled and factorized the matrix in (10).

Computation of the modal parameters in the finite element context

- compute the discrete eigenvectors w_1^h and w_2^h using the EB12 code;
- compute the ratio p/q from (20);
- compute the discrete Hessian $\underline{\underline{\varrho}}_1^h$ and $\underline{\underline{\varrho}}_2^h$ using the variational equation $(12)_1$ with $w = w_1^h$ and $w = w_2^h$;
- solve (8) for $\psi_{i,j}^h$ where the source term is successively $[w_i^h, w_j^h] = [[\underline{\underline{\varrho}}_i^h, \underline{\underline{\varrho}}_j^h]]$, for $i, j = 1, 2$;
- compute the ratios b/c and b/a from (20);
- compute the modal parameters using (20).

Some remarks are in order. Firstly, observe that we have to compute the Hessian through the weak formulation because, the eigenvectors not being in H^2, the second-order derivatives are not available. Secondly, it is important to remark that only two matrices are involved here: the matrix of system (8) and the mass matrix used to recover the three components of the tensors in $(12)_1$ where some attention must be paid to the boundary conditions imposed on these components. In fact, in the $I(\phi)$ and $II(\phi)$ cases, where the computation of $\psi_{i,j}$ is decoupled from that of the Airy stress, we may replace the matrix of (8) by that of a Dirichlet or Neumann problem as the case dictates. Doing so, the storage requirement decreases. However, if one does so in the $II(\phi)$ case, one should keep in mind that to fix the arbitrary constant in $\psi_{i,j}$, the only acceptable choice is the one for which the resulting solution has zero average over Ω.

5 Numerical results

We finally come to the presentation of the numerical results. As described earlier, these were obtained with the help of various finite element codes and EB12, which were all written in FORTRAN 77. These were run on two types of Unix machines: Sun workstations for the development and testing, and a SGI Power Challenge for the heavy computations of the eigenquantities and the bifurcation diagrams. In view of the dominant role of symmetry, all the computations were

conducted on meshes for which the discrete solutions exhibit the same symmetries as those of the solution of the continuous problem. These meshes were easily constructed by first partitioning the computation domain in equal subsquares which were then split into four equal triangles using the diagonals. In the first two sections, the computation domain was the unit square $[0, 1]^2$ and the mesh resulting from a partition in n^2 subsquares (hence in $4n^2$ elements) will be denoted by $M(n)$. Also, to distinguish the various symmetries, in the following we shall call 'even' the solutions w for which

$$w\left(\frac{l}{2}-a, y\right)=w\left(\frac{l}{2}+a, y\right)$$

and 'odd' those for which

$$w\left(\frac{l}{2}-a, y\right)=-w\left(\frac{l}{2}+a, y\right)$$

where $a \in [0, l/2]$.

5.1 Determination of the critical length and the dominant modes

Our spectral code based on the EB12 subroutine was used to determine both the critical length and the corresponding eigenvectors of (6). The computation of such lengths has been conducted in Schaeffer and Golubitsky (1979), for the $I(u)$ case in which, for each wavenumber k, the critical length is $\sqrt{k(k+1)}$, and in the $II(u)$ case in which it is $\sqrt{k(k+2)}$. Moreover, the eigenvectors are then known analytically. It will be useful to recall the behavior of those eigenvectors as functions of the length. For a small l, the dominating eigenvector, i.e. the one associated with the smalles eigenvalue, is even with one local extremum on the line $y=\frac{1}{2}$, while the second is odd with two symmetric extrema. When l reaches its first critical value the dominant eigenvalue is double and both eigenvectors are in the eigenspace. If l increases slightly, the eigenvectors exchange their role and the odd one becomes dominant. As l further increases, the $k=1$ mode disappears and is replaced by an even mode with three extrema. At the next critical value, there is another exchange and so forth.

This information is crucial. Indeed, numerical approximation is such that one cannot hope to obtain a perfect double eigenvalue for any length and the best that we can hope for is to locate the critical values in small intervals. This is done in an indirect way: as the length is varied with a fixed step Δl, the two dominant eigenvalues and eigenvectors are computed with the help of EB12 and the value of the dominant mode at $(l/2, 1/2)$ is printed. If it is near zero the mode is odd, otherwise it is even. If, for two successive values of l, the dominant modes have exchanged their position, a simple continuity argument shows that the eigenvalues must have coincided for an intermediate value of the length. If the increment Δl is too big, it is decreased and the computation is restarted from the last value of l. We shall say that the eigenvalue is double when the approximations agree to four significant digits. The corresponding length is then called critical and the two eigenvectors are stored for future purposes.

One reason why this calculation is time consuming is that, to obtain a good approximation of the two eigenvalues and eigenvectors, we have to compute more than two of them. Typically, we have been looking for an eigenspace of dimension 8, using 50 guard vectors (see Duff & Scott, 1991, for the technical details). This

Table 1.

	$I(\phi)$			$II(\phi)$		
	μ	ν	$\mu\nu$	μ	ν	$\mu\nu$
$M(8)$	3.143	1.264	3.961	4.796	1.192	5.715
$M(16)$	3.098	1.267	3.925	4.800	1.119	5.753
$M(32)$	3.807	1.267	3.917	4.802	1.200	5.763
H–S	3.804	1.269	3.915	4.802	1.201	5.767

large number of guard vectors increased the storage requirements quite a bit, but, conversely, it enhanced convergence significantly thus reducing the number of matrix vector multiplications which is the costliest operation. Since, according to Duff and Scott (1991), it is hard to determine the numerical parameters for EB12 in advance, our choice was based on trial and error.

To validate our approach, let us consider the $I(u)$ case, and compare the value of the first critical length ($k = 1$) obtained by this approach to the analytical value $l_c = \sqrt{2}$. On the $M(16)$ mesh, we obtain the approximation $l_c = 1.4142$ and the same value on $M(32)$. This is very satisfactory.

Turning our attention to the case of a clamped plate ($III(u)$), we first remark that no analytic expression is known for the eigenvalues or the eigenvectors and this is irrespective of the plate size. Moreover, as far as we know, the possible appearance of a double eigenvalue has never been discussed. This is why we built the code but, in absence of a firmer theoretical basis, the reader should look upon our numerical results as indications, albeit precise, of the behavior of the continuous system. Even if we have computed the critical length for the first wavenumbers, we shall limit our attention to the case $k = 5$, which corresponds to Stein's experiment. In that case, the application of our methodology gives the approximation $l_c \simeq 3.927$ on the $M(16)$ mesh, the approximation $l_c \simeq 3.912$ on the $M(32)$ mesh and the same one (up to four digits) on the $M(40)$ mesh. This is the value that we have kept. The corresponding numerical buckling load is $\lambda = 71.34$ and the shape of the eigenvectors is illustrated in Fig. 5 which shows a cut of the graph along the line $y = \frac{1}{2}$ (we recall that the computational domain is the unit square).

5.2 Computation of the modal parameters

The critical length and corresponding eigenvectors being available, we can now use the algorithm presented in Section 3 to compute the modal parameters. Even if, in the $I(\phi)$ and $II(\phi)$ cases, the inverse bilaplacian can be factorized, we have made most of the computations of the $\psi_{i,j}$ using our psi–omega code. Only when memory requirements were becoming stringent did we resort to a simpler Neumann code. Of course, when comparisons were possible and valid, both codes gave the same results. In all the following computations, even when we refined the mesh, we used as critical length either the analytical value or the converged numerical one. The computed eigenvectors were then considered as approximations of the exact ones.

5.2.1 Validation. The validation of our numerical approach is based on a comparison with the numerical results presented in Holden and Schaeffer (1984). It

must be recalled that, in the $I(u)-II(\phi)$ and $II(u)-II(\phi)$ cases, those results were in complete agreement with the analytical results obtained in Schaeffer and Golubitsky (1979).

Table 1 presents a comparison between our results (rounded to three digits), obtained on three successively refined meshes, and those of Holden and Schaeffer (H–S) (1984) in the $I(u)$, $k = 1$ case. The quality of the approximation is obvious. However, if we increase k the problem seems to become stiffer and finer meshes

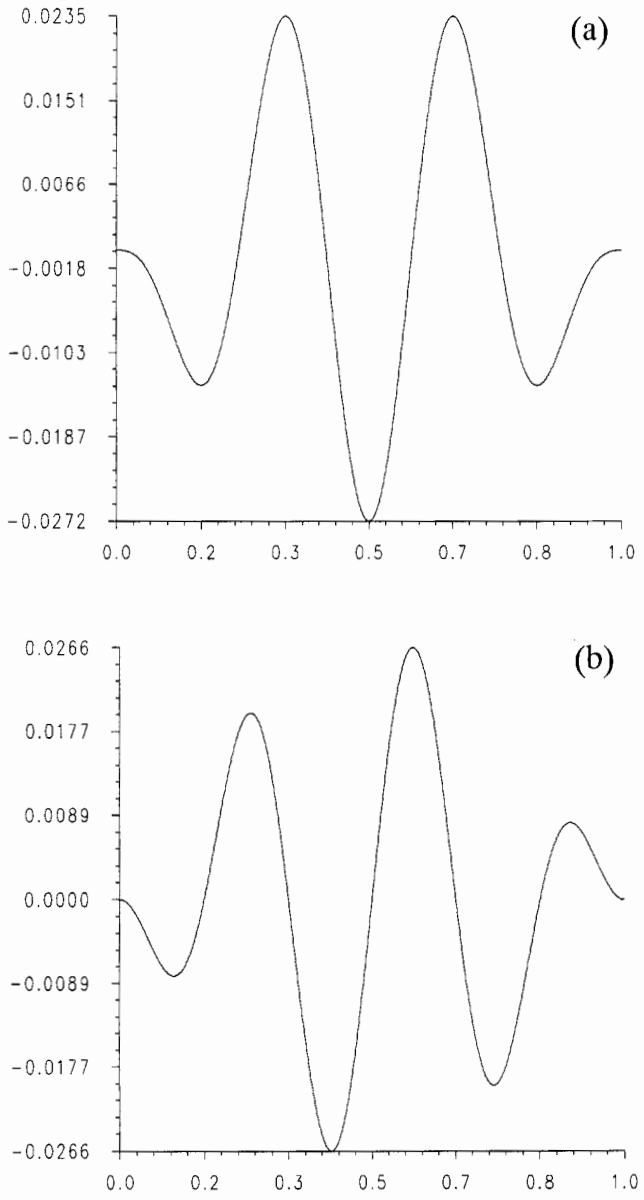

Fig. 5. The eigenvectors.

Table 2.

	$I(\phi)$			$II(\phi)$		
	μ	ν	$\mu\nu$	μ	ν	$\mu\nu$
$M(16)$	1.081	0.968	1.046	1.486	1.350	2.008
$M(32)$	1.053	0.9864	1.038	1.077	0.961	1.036
$M(40)$	1.050	0.9881	1.037	1.077	0.963	1.032
H–S	1.046	0.991	1.037	1.086	0.971	1.055

are needed. As a second example, we consider the case $II(u)$, $k=5$ which corresponds to Stein's experiment (Table 2).

In both cases the approximations on the finest mesh are within 1% of the value obtained by Holder and Schaeffer. However, on $M(16)$ the predicted behavior of the discrete solution in the $II(\phi)$ case is wrong, which illustrates the necessity of validating the predictions by mesh refinements. There could be cases where this is impossible because of the cost associated with the computation of the eigenvectors. However, in the $I(u)$ and $II(u)$ cases, we can replace those computed by EB12 by the interpolate of the exact eigenvectors on the mesh at hand, since they give another convergent approximation. If we do that in the $II(\phi)$ case, the values of the parameters on $M(64)$ are $\mu=1.081$, $\nu=0.967$ and $\mu\nu=1.046$. This is better than the other approximation on $M(40)$ but could still be improved. We believe that the difficulty here stems from the compatibility condition. Since, in the computation of $\psi_{i,j}$,

$$\int_{\Omega} [[\sigma_{w_{h,i}}, \sigma_{w_{h,i}}]] \, d\underline{x} \neq 0$$

we have to project the right-hand side of the corresponding system (8) on L_0^2. This process is convergent but the convergence is slow. To improve upon it, we would need a better approximation of the Poisson bracket which is not available at a low cost. This will be general: Neumann boundary conditions are harder to treat than Dirichlet ones and the convergence with mesh refinement is always slower in the $II(\phi)$ case than in the other two.

5.2.2 New results. Before turning our attention to the case of a clamped plate ($III(u)$), we consider the possibility of using the boundary conditions $III(\phi)$ in

Table 3.

	$I(u)$			$II(u)$		
	μ	ν	$\mu\nu$	μ	ν	$\mu\nu$
$M(16)$	2.317	1.726	4.0	1.075	0.9726	1.048
$M(32)$	2.171	1.811	3.932	1.056	0.9847	1.041
$M(40)$	2.159	1.817	3.925	1.055	0.9857	1.040
H–S($I(\phi)$)	2.055	1.820	3.740	1.046	0.991	1.037
H–S($II(\phi)$)	3.541	2.459	8.707	1.086	0.971	1.055

Table 4.

	$I(\phi)$			$II(\phi)$			$III(\phi)$		
	μ	v	μv	μ	v	μv	μ	v	μv
$M(16)$	1.113	0.9393	1.046	1.282	1.194	1.530	1.094	0.9570	1.047
$M(32)$	1.052	0.9834	1.035	1.055	0.9838	1.038	1.056	0.9847	1.037
$M(40)$	1.048	0.9866	1.034	1.053	0.9831	1.035	1.053	0.9847	1.037

combination with $I(u)$ and $II(u)$. Here again, we shall give results for the $k = 5$ case and compare them to those obtained by Holder and Schaeffer (1984) with the other two sets of boundary conditions (Table 3). Looking at these results, one first notices that the numerical values seem to converge with mesh refinement. Next, it appears that the replacement of the boundary conditions $I(\phi)$ by $III(\phi)$ does not alter the values of the modal parameters very much. Finally, and more importantly, in these two cases, the predicted qualitative behavior of the plate does not seem to depend on the choice of boundary conditions for the Airy stress.

The above observation suggests that, in the $III(u)$ case, it is interesting to compare the results obtained with the three sets of boundary conditions for ϕ. This comparison is presented in Table 4.

Convergence with mesh refinement is satisfactory and, as before, on the finest mesh the predicted behavior is the same for the three sets of boundary conditions. However, on the $M(16)$ mesh, the choice $II(\phi)$ leads to the wrong answer. This confirms the fact that, with this set of boundary conditions, the problem is stiffer.

Remark 1. The above computations suggest that the boundary conditions on the stress potential do not influence the appearance of mode jumping. If this was true, it would be interesting since the boundary conditions $I(\phi)$ and $III(\phi)$ are much easier to implement than $II(\phi)$. However, preliminary computations in the case of a plate compressed on its four sides (a case considered, for example, in Reinhart, 1982) seem to indicate that this might not be true in general.

Similarly, in the above examples, the post-buckling behavior seems to be independent of the wavenumber of the first bifurcated solution. Again, the situation appears to be different for a compression applied on the whole boundary. In fact, the general behavior is much more complicated in that case and we hope to come back to this in the near future.

5.3 The bifurcation diagrams

To conclude, we come back to some of the new results presented in the preceding sections. To validate these, we have performed a direct simulation using the perturbation–continuation algorithm described in Section 3.3. The graphical representation of the resulting diagram calls for the selection of an indicator which correctly represents the behavior of the solution. Since the bifurcations are caused by symmetry breaking, we have chosen

$$f(\lambda) = u\left(\frac{l}{2}, \frac{l}{2}\right) + \frac{\partial u}{\partial x}\left(\frac{l}{2}, \frac{l}{2}\right)$$

This indicator satisfies the basic symmetry property with respect to the plane of the plate, in particular, on the trivial branch, $f = 0$. On the branch of even

solutions, only the first term counts while on the branch of odd solutions it is the second which gives the information.

Although the bifurcation branches should, *a priori*, be drawn in a three-dimensional (30) space, we have projected them on to a plane. While the qualitative behavior can still be distinguished, the reader should be warned that some intersection points of the two-dimensional (2D) representation are artificial, in the sense that they do not correspond to a 3D phenomenon.

In all cases, the simulation has been conducted on a fixed symmetric mesh for which the relevant parameters are:

- total number of elements = 1764;
- total number of nodes = 3645.

Since we have roughly eight unknowns per node, the determination of the birfurcation diagram required the resolution of a parameterized discrete nonlinear system of more than 25 000 equations (the precise figure depends on the boundary conditions). We usually worked with a fixed load step $\Delta\lambda$, which was sometimes adjusted in the neighborhood of a critical point. The detection of the bifurcation values on the various branches was based on the criterion presented in Allgower and George (1990, Section 8.1) which states that, at a simple bifurcation point, the determinant of the matrix of the extended system changes sign. If this extended matrix is written

$$\mathbf{H} = \begin{pmatrix} A & b \\ c^t & d \end{pmatrix}$$

it can be factorized as

$$\mathbf{H} = \begin{pmatrix} A & 0 \\ c^t & d - c^t A^{-1} b \end{pmatrix} \begin{pmatrix} 1 & A^{-1} b \\ 0 & 1 \end{pmatrix}$$

Since our linear solver is built upon this factorization (see Keller, 1977), the computation of the determinant sign was just a by-product which did not require much extra work.

5.3.1 The simply supported plate: $I(u)$, $III(\phi)$, $k = 5$. In this first case, the critical values $l_c = \sqrt{30}$ and

$$\lambda_c = \pi^2 \frac{(25 + l_c^2)^2}{25 l_c^2} = 39.8074$$

are known. Using $l = 5.4$, we have obtained the diagram shown as Fig. 6. The bifurcation to the even solutions occurs on the interval $\lambda \in [39.72, 39.73]$ and the bifurcation to the odd solutions occurs on $\lambda \in [39.93, 39.94]$. This is in good agreement with the theory.

Following the branch of odd solutions, we found a secondary bifurcation in [40.106, 40.195]. Switching on the branch of mixed solutions, we followed it, in both directions, until past $\lambda = 80$ without meeting another bifurcation. This suggests that no mode jumping is taking place as was predicted by the value of the modal parameters shown in Table 3. Similarly, we went back to the basic branch, switched on to that of even solutions and followed it as far as before: still no bifurcation. Thus, it seems reasonable to believe that, with the boundary conditions $I(u)$, $III(\phi)$, the system behaves in the same way as with $I(u)$, $I(\phi)$ and $I(u)$, $II(\phi)$, in the sense that there is no mode jumping.

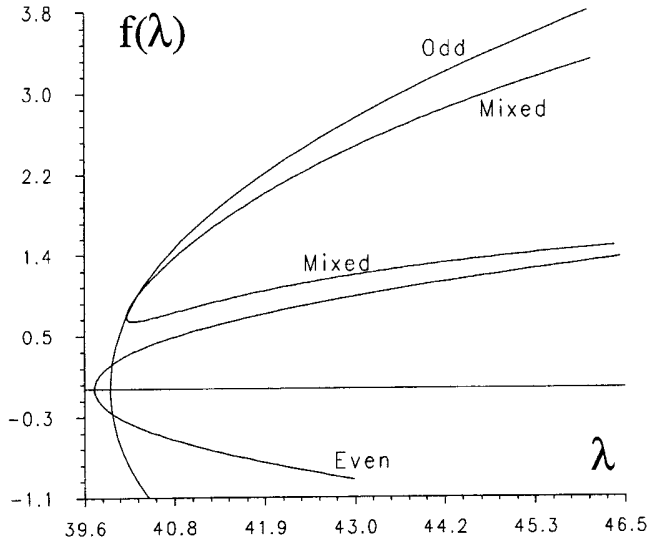

Fig. 6. Simply supported plate.

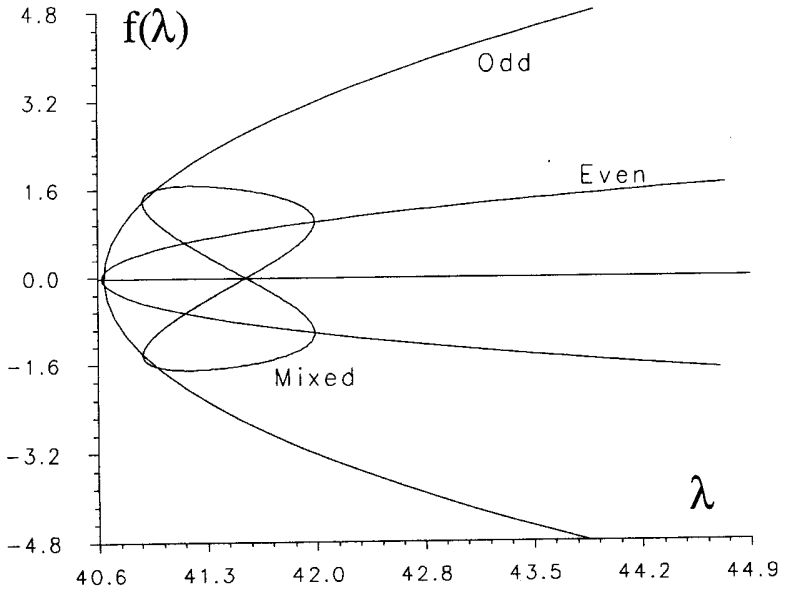

Fig. 7. Partly clamped plate.

5.3.2 The partly clamped plate: II(u), III(φ), k = 5. In this second case, the critical values $l_c = \sqrt{35}$ and

$$\lambda_c = \frac{\pi^2}{l_c^2}(2k^2 + 4k + 4) + 2\pi^2 = 40.6064$$

are also known. Using $l = 5.9$, we have obtained Fig. 7. The bifurcation to the even solutions occurs on the interval $\lambda \in [40.620, 40.624]$ and the bifurcation to the odd solutions occurs on $\lambda \in [40.636, 40.640]$, which is in very good agreement with the theory.

Following the branch of odd solutions, we found the secondary bifurcation in [40.894, 41.025]. Switching on the branch of mixed solution, we followed it all the way back. Doing so, we first crossed the branch of even solutions for $\lambda \in [41.883, 42.089]$ and then the two same branches for the same values of λ and symmetric values of f. Not only does this confirm that mode jumping is taking place in the $III(\phi)$ case, but the geometry suggests that, as in the case of $I(\phi)$ and $II(\phi)$, the branch of mixed solutions is unstable.

5.3.3 The clamped plate: III(u), III(φ), k = 5. In this third case, the approximate critical values are $l_c = 3.912$ and $\lambda_c = 71.34$. Using $l = 3.9$, we have obtained Fig. 8. This time, the bifurcation to the even solutions occurs on the interval $\lambda \in [71.690, 71.691]$ and the bifurcation to the odd solutions occurs on $\lambda \in [71.707, 71.708]$, while the secondary bifurcation on the branch of odd solutions has been detected in [72.02, 72.08]. We have again followed the mixed branch until it looped back and observed that the crossings with the branch of even solution are at $\lambda \in [73.26, 73.29]$. As to the stability issue, it appears that the mode-jumping phenomenon observed in this case is qualitatively equivalent to that observed previously.

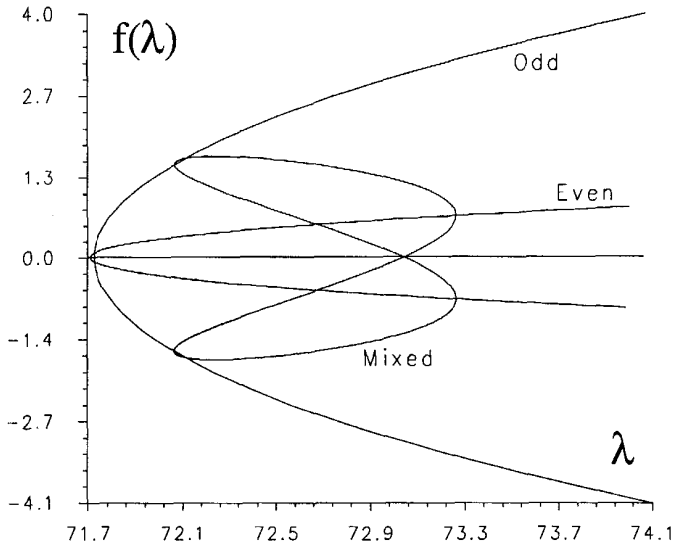

Fig. 8. Fully clamped plate.

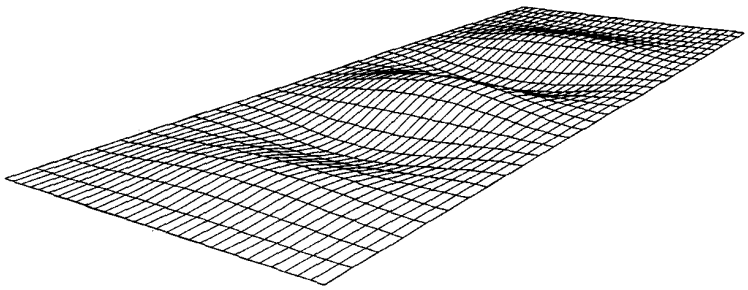

(a)

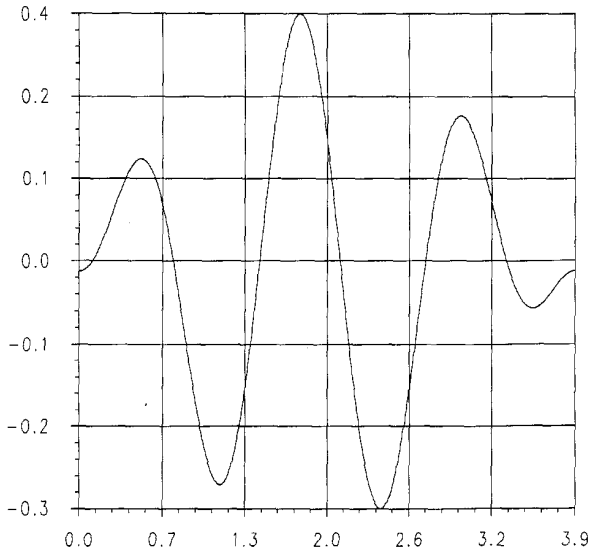

(b)

Fig. 9. Mixed solution, $\lambda \approx 72.14$.

In conclusion, we offer a view of the changes in shape of the mixed solution, along the branch which starts on the odd one and ends on the even one (Figs 9 and 10).

6 Conclusions

In this paper, we have shown how to combine a finite element discretization, the subspace iteration method, the continuation procedure of Keller and the analysis of Schaeffer and Golubitsky, to complete the study of the post-buckling behavior of a rectangular plate subject to a longitudinal compression. The set of tools that we have developed allows for a complete analysis: computation of the spectral quantities, determination of the bifurcation diagrams and computation of the modal parameters. Using these, we were able to show that the mode-jumping phenomenon can also be observed with a fully clamped plate and that, in the case considered by Schaeffer and Golubitsky (1979), the choice of the boundary

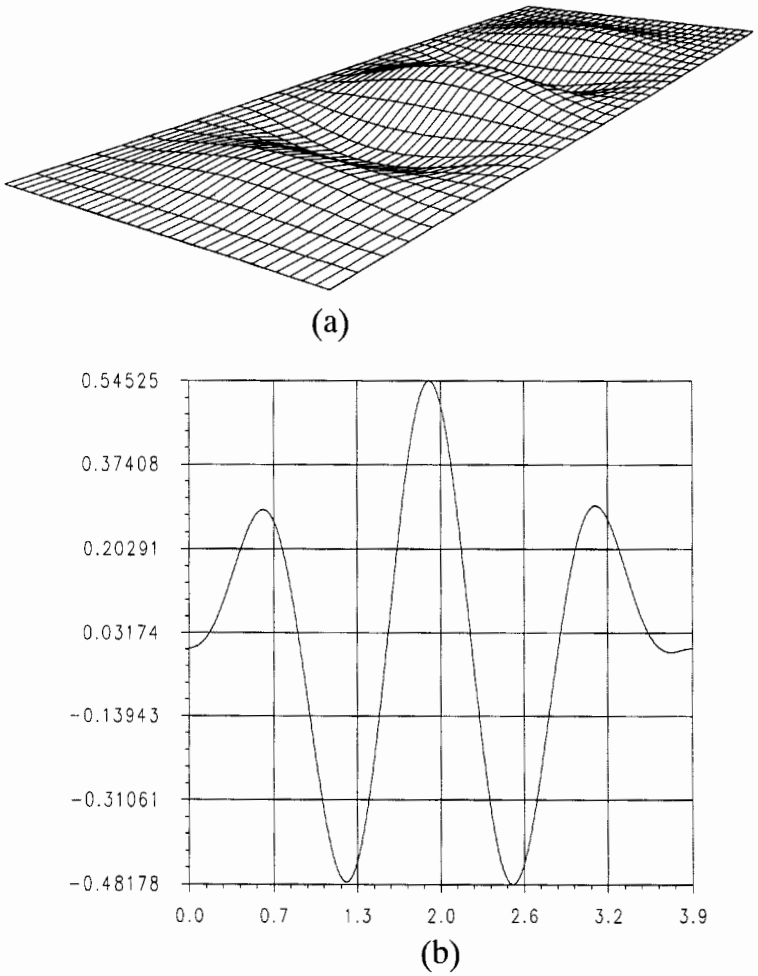

Fig. 10. Mixed solution, $\lambda = 72.66$.

conditions on the Airy stress does not seem to matter when one is interested in the qualitative behavior of the plate.

Acknowledgements

The authors would like to thank one of the referees for pointing out the reference by Riks *et al.* (1996). They also warmly thank Mr Kokou Dossou who collaborated in the compuation of the bifurcation diagrams.

References

Allgower, E. G. and Georg, K. (1990) *Numerical Continuation Methods*, Springer Series in Computational Mathematics, 13 (Springer, Berlin, Heidelberg).

Babŭska, I and Osborn, J. (1991) Eigenvalue problems. *Handbook of Numerical Analysis*, Vol. II, Part 1 (eds P. G. Ciarlet and J. L. Lions; Elsevier Science, North Holland, Amsterdam), pp. 642–787.

Bauer, L., Keller, H. and Reiss, E. (1975) Multiple eigenvalues lead to secondary bifurcation. *SIAM Journal of Applied Mathematics* **17**, 101–122.

Berger, M. S. and Fife, P. C. (1968) von Kármán equations and the buckling of a thin elastic plate II. Plate with general edge conditions. *Communications in Pure and Applied Mathematics* **21**, 227–241.

Brezzi, F., Rappaz, J. and Raviart, P. A. (1980–1981) Finite dimensional approximations of nonlinear problems. Part I: branches of nonsingular solutions. *Numerical Mathematics* **36**, 1–25. Part II: limit points. *Numerical Mathematics* **37**, 1–28. Part III: simple bifurcation points. *Numerical Mathematics* **38**, 1–30.

Ciarlet, P. G. and Rabier, P. (1980) Les équations de von Kármán. *Lecture Notes in Mathematics* **826**, (Springer, New York).

Duff, I. and Scott, J. (1991) Computing selected eigenvalues of sparse unsymmetric matrices using subspace iteration. *ACM Transactions in Mathematical Software* **19**, 13–159.

Falk, J. and Osborn, J. (1980) Error estimates for mixed methods. *R.A.I.R.O. Analyse Numérique* **14**, 249–277.

Glowinski, R., Keller, H. and Reinhart, L., (1985) Continuation–conjugate gradient methods for the least square solution of nonlinear boundary value problems. *SIAM Journal on Scientific and Statistical Computing* **6**, 793–832.

Golubitsky, M. and Schaeffer, D. (1985) *Singularity and Groups in Bifurcation Theory*, Vol. 1, Applied Mathematical Sciences **51** (Springer, New York).

Holder, E. J. and Schaeffer, D. (1984) Boundary conditions and mode jumping in the von Kármán equations. *SIAM Journal of Mathematical Analysis* **15**, 446–458.

Keller, H. B. (1977) Numerical solution of bifurcation and nonlinear eigenvalue problems. *Applications of Bifurcation Theory* (eds Paul. H. Rabinowtiz; Academic Press, New York).

Miyoshi, T. (1976) A mixed finite element method for the solution of the von Kármán equations. *Numerical Mathematics* **26**, 255–269.

Oukit, A. and Pierre, R. (1996) Mixed finite element for the linear plate problem: the Hermann–Miyoshi model revisited. *Numerical Mathematics* **74**, 453–477.

Potier-Ferry, M. (1978) Bifurcation et stabilité pour des systèmes dérivant d'un potentiel. *Journal de Mécanique* **17**, 579–608.

Reinhart, L. (1982) On the numerical analysis of the von Kármán equations: mixed finite element approximation and continuation techniques. *Numerical Mathematics* **39**, 371–404.

Riks, E., Rankin, C. and Brogan, F. A. (1996) On the solution of mode jumping phenomena in thin walled structures. *Computer Methods in Applied Mechanics and Engineering* **136**, 59–92.

Schaeffer, D. and Golubitsky, M. (1979) Boundary conditions and mode jumping in the buckling of a rectangular plate. *Communications in Mathematical Physics* **69**, 209–236.

Stein, M. (1959) The phenomenon of change of buckle patterns in elastic structures. Nasa Technical Report, R-39.